An ALMA survey of submillimetre galaxies in the Extended *Chandra Deep Field*-South: detection of [C II] at $z = 4.4$

A. M. Swinbank,[1][*] A. Karim,[1] Ian Smail,[1] J. Hodge,[2] F. Walter,[2] F. Bertoldi,[3]
A. D. Biggs,[4] C. de Breuck,[4] S. C. Chapman,[5] K. E. K. Coppin,[6] P. Cox,[7]
A. L. R. Danielson,[1] H. Dannerbauer,[8] R. J. Ivison,[9,10] T. R. Greve,[11] K. K. Knudsen,[12]
K. M. Menten,[14] J. M. Simpson,[1] E. Schinnerer,[2] J. L. Wardlow,[13] A. Weiß[14]
and P. van der Werf[15]

[1]*Institute for Computational Cosmology, Durham University, South Road, Durham DH1 3LE*
[2]*Max-Planck-Institut für Astronomie, Königstuhl 17, D-69117 Heidelberg, Germany*
[3]*Argelander-Instutute of Astronomy, Bonn University, Auf dem Huegel 71, D-53121 Bonn, Germany*
[4]*European Southern Observatory, Karl-Schwarzschild Strasse 2, D-85748 Garching, Germany*
[5]*Institute of Astronomy, University of Cambridge, Madingley Road, Cambridge CB3 0HA*
[6]*Department of Physics, McGill University, 3600 Rue University, Montréal, QC H3A 2T8, Canada*
[7]*Institut de Radioastronomie Millimètrique, 300 rue de la piscine, F-38406 Saint-Martin d'Hères, France*
[8]*Universität Wien, Institut für Astrophysik, Türkenschanzstraße 17, 1180 Wien, Austria*
[9]*UK Astronomy Technology Centre, Science and Technology Facilities Council, Royal Observatory, Blackford Hill, Edinburgh EH9 3HJ*
[10]*Institute for Astronomy, University of Edinburgh, Blackford Hill, Edinburgh EH9 3HJ*
[11]*Department of Physics & Astronomy, University College London, Gower Street, London WC1E 6BT*
[12]*Department of Earth and Space Sciences, Chalmers University of Technology, Onsala Space Observatory, SE-43992 Onsala, Sweden*
[13]*Department of Physics & Astronomy, University of California, Irvine, CA 92697, USA*
[14]*Max-Planck-Institute für Radioastronomie, Auf dem Hugel 69, D-53121 Bonn, Germany*
[15]*Leiden Observatory, Leiden University, PO Box 9513, 2300 RA Leiden, Netherlands*

ABSTRACT

We present Atacama Large Millimeter Array (ALMA) 870-µm (345-GHz) observations of two submillimetre galaxies (SMGs) drawn from an ALMA study of the 126 submillimetre sources from the LABOCA Extended *Chandra Deep Field*-South Survey (LESS). The ALMA data identify the counterparts to these previously unidentified submillimetre sources and serendipitously detect bright emission lines in their spectra which we show are most likely to be [C II] 157.74 µm emission yielding redshifts of $z = 4.42$ and 4.44. This blind detection rate within the 7.5-GHz bandpass of ALMA is consistent with the previously derived photometric redshift distribution of SMGs and suggests a modest, but not dominant ($\lesssim 25$ per cent), tail of 870-µm selected SMGs at $z \gtrsim 4$. We find that the ratio of $L_{[C II]}/L_{FIR}$ in these SMGs is much higher than seen for similarly far-infrared-luminous galaxies at $z \sim 0$, which is attributed to the more extended gas reservoirs in these high-redshift ultraluminous infrared galaxies (ULIRGs). Indeed, in one system we show that the [C II] emission shows hints of extended emission on $\gtrsim 3$ kpc scales. Finally, we use the volume probed by our ALMA survey to show that the bright end of the [C II] luminosity function evolves strongly between $z = 0$ and ~ 4.4, reflecting the increased interstellar medium cooling in galaxies as a result of their higher star formation rates. These observations demonstrate that even with short integrations, ALMA is able to detect the dominant fine-structure cooling lines from high-redshift ULIRGs, measure their energetics and spatially resolved properties and trace their evolution with redshift.

Key words: galaxies: evolution – galaxies: high-redshift – galaxies: starburst.

1 INTRODUCTION

A significant fraction of the obscured star formation at $z \gg 1$ arises from the most luminous galaxies (e.g. Blain et al. 1999; LeFloc'h et al. 2009): ultraluminous infrared galaxies (ULIRGs; Sanders &

Mirabel 1996) with bolometric luminosities of $\gtrsim 10^{12}$–10^{13} $L_\odot$ and star formation rates $\gtrsim 100$–$1000\,M_\odot\,yr^{-1}$. At high redshift, these galaxies are some of the brightest sources in the submillimetre waveband and so are frequently called 'submillimetre galaxies' (SMGs).

The spectral energy distribution (SED) of the dust emission in these luminous dusty galaxies has a Rayleigh–Jeans tail that produces a negative *K*-correction in the submillimetre waveband, yielding a near-constant flux density–luminosity dependence with redshift over the range $z \sim 1$–6 (Blain et al. 2002). Although the volume density of the SMG population evolves rapidly with redshift (showing a 1000-fold increase in the space density over $\sim 10\,Gyr$ to $z \sim 2.5$; Chapman et al. 2005), the volume density appears to subsequently decline above $z \gtrsim 3$. This decline is not a result of a reduction in their apparent flux density in the submillimetre, but a real reduction in the volume density of SMGs (Wardlow et al. 2011).

However, determining the precise strength of the decline in the SMG volume density requires locating the counterparts of high-redshift SMGs. This is problematic due to the poor resolution of single dish submillimetre maps, which means that SMGs have to be identified through correlations between their submillimetre emission and that in other wavebands where higher spatial resolution is available (usually the radio and/or mid-infrared; e.g. Ivison et al. 2002; Chapman et al. 2004; Pope et al. 2006; Ivison et al. 2007). These identifications are probabilistic as they rely on empirical correlations that both have significant scatter and may evolve with redshift (e.g. Carilli & Yun 2000). Moreover, the SEDs in these other wavebands have positive *K*-corrections and hence can miss the highest redshift counterparts. Indeed, in submillimetre surveys typically 30–50 per cent of SMGs lack 'robust' counterparts in the radio or mid-infrared, and these may represent an unidentified tail of high-redshift SMGs (e.g. Biggs et al. 2011; see also Lindner et al. 2011). To circumvent this problem requires identifying SMGs using (sub)millimetre interferometers (e.g. Frayer et al. 2000; Gear et al. 2000), but until recently their sensitivity has been too low to locate large number of SMGs (e.g. Dannerbauer et al. 2002; Younger et al. 2007; Wang et al. 2011; Smolčić et al. 2012). However, with the commissioning of the Atacama Large Millimeter Array (ALMA), we can now construct the large samples of precisely located SMGs needed to unambiguously study their properties and test galaxy formation models.

Whilst the bulk of the bolometric emission from SMGs is radiated through continuum emission from dust grains in the rest-frame far-infrared, superimposed on this are a series of narrow atomic and molecular emission lines. By far the strongest of these arise from the atomic fine-structure transitions of carbon, nitrogen and oxygen in the far-infrared, along with weaker, but more commonly studied molecular lines visible at millimetre wavelengths (e.g. ^{12}CO, HCN). These bright emission lines are an important pathway by which the dense gas in these galaxies cools, and so provide a unique tracers of the star formation process in these galaxies.

The brightest and best studied of the atomic lines in the far-infrared is the $^2P_{3/2}$–$^2P_{1/2}$ fine-structure line of singly ionized carbon at 157.74 μm (hereafter [C II]). Much of the [C II] emission from galaxies arises from the warm and dense photodissociation regions (PDRs) that form on the ultraviolet (UV) illuminated surface of molecular clouds, although the [C II] flux from diffuse H II regions or from cool, diffuse interstellar gas can also be significant (e.g. Madden et al. 1993; Lord et al. 1996). The [C II] emission line therefore provides an indication of the gas content and the extent of the gas reservoir in a galaxy. Far-infrared surveys of low-redshift

galaxies from the *Kuiper Airborne Observatory* and *Infrared Space Observatory* (*ISO*) have shown that the [C II] line can comprise $\gtrsim 1$ per cent of the total bolometric luminosity (Stacey et al. 1991; Brauher, Dale & Helou 2008; Graciá-Carpio et al. 2011). This bright line is thus ideally suited for deriving redshifts for obscured galaxies and investigating their dynamics and star formation properties.

Early searches for [C II], by necessity, focused on the highest redshift far-infrared sources, $z > 4$, where the [C II] line is shifted into the atmospheric windows in the submillimetre (e.g. Ivison, Harrison & Coulson 1998; Maiolino et al. 2005, 2009; Wagg et al. 2010). Most of these sources host powerful active galactic nuclei (AGN; as well as being ULIRGs), and it was noted that their [C II] lines were weak relative to L_{FIR}, demonstrating the same behaviour as seen in AGN-dominated ULIRGs in the local Universe. However, more recent observations of the [C II] emission in high-redshift star-formation-dominated ULIRGs have shown that the [C II] emission can be as bright as in local, low-luminosity galaxies, $L_{[C II]}/L_{FIR} \sim 0.1$–1 per cent (e.g. Hailey-Dunsheath et al. 2008; Ivison et al. 2010b; Stacey et al. 2010; Valtchanov et al. 2011). This has been interpreted as due to the lower ionization field arising from more widely distributed star formation activity within these systems, in contrast to the compact nuclear star formation seen in low-redshift ULIRGs (e.g. Sakamoto et al. 2008). The strength of [C II] (and other atomic lines) and its relative strength to the far-infrared luminosity can therefore be used to probe the physical properties of the interstellar medium (ISM) in high-redshift galaxies.

We have recently undertaken an ALMA Cycle 0 study at 870 μm (345 GHz) of the 126 submillimetre sources located in the $0°.5 \times 0°.5$ LABOCA Extended *Chandra Deep Field*-South Survey ('LESS'; Weiß et al. 2009), the most uniform submillimetre survey of its kind to date. These ALMA data yield unambiguous identifications for a large fraction of the submillimetre sources, directly pinpointing the SMG responsible for the submillimetre emission to within <0.2 arcsec (Hodge et al., in preparation), without recourse to statistical radio/mid-infrared associations. In this paper, we present ALMA observations of two of the SMGs from our survey for which we are able to derive their redshifts from serendipitous identification of the [C II] emission line in the ALMA data cubes. We use the data to measure the energetics of the dominant fine-structure lines, to search for spatially resolved velocity structure and to provide an estimate of the evolution of the [C II] luminosity function with redshift. We adopt a cosmology with $\Omega_\Lambda = 0.73$, $\Omega_m = 0.27$ and $H_0 = 72\,km\,s^{-1}\,Mpc^{-1}$ in which 1 arcsec corresponds to a physical scale of 6.7 kpc at $z \sim 4.4$.

2 OBSERVATIONS AND REDUCTION

Observations of the 126 submillimetre sources in the LESS survey were obtained with ALMA at 345 GHz (Band 7) with a dual polarization set-up in the compact configuration, yielding a synthesized beam of $\sim 1.8 \times 1.2\,arcsec^2$. Our observations cover 7.5-GHz bandwidth, split between the upper and lower sidebands, 336.1–339.8 and 348.1–351.9 GHz. The observations employed 15 antennas, and data for these two sources were obtained between 2011 October and November in good conditions, precipitable water vapour (PWV) $\lesssim$ 0.5 mm. The primary beam of the ALMA dishes, ~ 18 arcsec full width at half-maximum (FWHM) at our observing frequency, is sufficient to encompass the error circles of the SMGs from the LESS maps, $\lesssim 5$ arcsec (Weiß et al. 2009), even in confused situations. The observing frequency was selected to match the original LABOCA discovery map to ensure that the ALMA and LABOCA flux

densities could be easily compared. Each galaxy was observed for a total of $\sim$120 s, with phase, bandpass and flux calibration based on J0403$-$360, J0538$-$440 and Mars, respectively. The data were processed with the Common Astronomy Software Application (CASA; McMullin et al. 2007), and we constructed both velocity-integrated maps and data cubes with 62.5-MHz (54.5 km s^{-1}) binning. The velocity-integrated continuum maps for the two sources discussed here reach noise levels of $\sigma = 0.44$ and 0.42 mJy beam^{-1} for LESS 61 and LESS 65, respectively. This is a factor of $\sim$3 times more sensitive than the original LABOCA discovery map, while more critically the beam is $\sim$150 times smaller in area than that of LABOCA (with a corresponding reduction in the positional uncertainty of detected sources). In the data cubes, the rms sensitivity is $\sim$3.8 mJy beam^{-1} per 54.5 km s^{-1} (62.5-MHz) channel. The full catalogue of the ALMA SMGs will be published in Hodge et al. (in preparation), whilst the ALMA 870-μm counts and multiwavelength properties of the ALMA SMGs will be published in Karim et al. (in preparation) and Simpson et al. (in preparation).

3 ANALYSIS AND DISCUSSION

Wardlow et al. (2011) derive a photometric redshift distribution for the statistically identified radio and mid-infrared counterparts of the LESS submillimetre sources, deriving a median $z = 2.5 \pm 0.5$. Taking the errors on the redshifts into account, we expect 3.5 ± 0.5 SMGs to have far-infrared fine-structure lines (such as [C II] 157.74 μm, [O I] 145 μm, [N II] 122 μm or [O III] 88 μm) within the 7.5-GHz bandwidth of ALMA. By far the brightest of these lines in local ULIRGs is the [C II] emission line, with a me-

dian equivalent width $\gtrsim$10 times brighter than any of the other lines (Brauher et al. 2008). Focusing just on [C II], we expect that 1.5 ± 0.5 SMGs in our sample will have detectable [C II] emission in the ALMA bandpass, with corresponding redshift ranges of $z = 4.399$–4.461 and 4.590–4.656 for the upper and lower sidebands.

As an initial step in our analysis of the ALMA maps of the LESS submillimetre sources, we exploit the frequency coverage of our observations to search for emission lines in the data cubes. For each $>4\sigma$ SMG in the velocity-integrated ALMA maps within the primary beam, we extract the spectra and search for emission lines by attempting to fit a Gaussian emission-line profile to the spectrum, only accepting the fit if $\Delta\chi^2$ provides a significant improvement ($\Delta\chi^2 > 25$ or $\sim5\sigma$) over a continuum-only fit.

3.1 Source identification

In two submillimetre sources, LESS J033245.6$-$280025 and LESS J033252.4$-$273527 [hereafter ALESS 61.1 and ALESS 65.1, respectively, following the notation in Hodge et al. (in preparation)], we identify bright emission lines with FWHM 230 ± 25 and 490 ± 35 km s^{-1}, respectively, in the spectra of these SMGs. The significance of the emission lines (integrated over the line) is signal-to-noise ratio (S/N) ~ 5.3 and 7.0 for ALESS 61.1 and ALESS 65.1, respectively. In Fig. 1 we show the velocity-integrated (continuum plus line) ALMA maps of ALESS 61.1 and ALESS 65.1. To highlight the emission-line detections in both ALMA SMGs, in Fig. 2 we also show the continuum-subtracted emission-line maps, while the spectra are shown in Fig. 3. In this figure, the map is made by
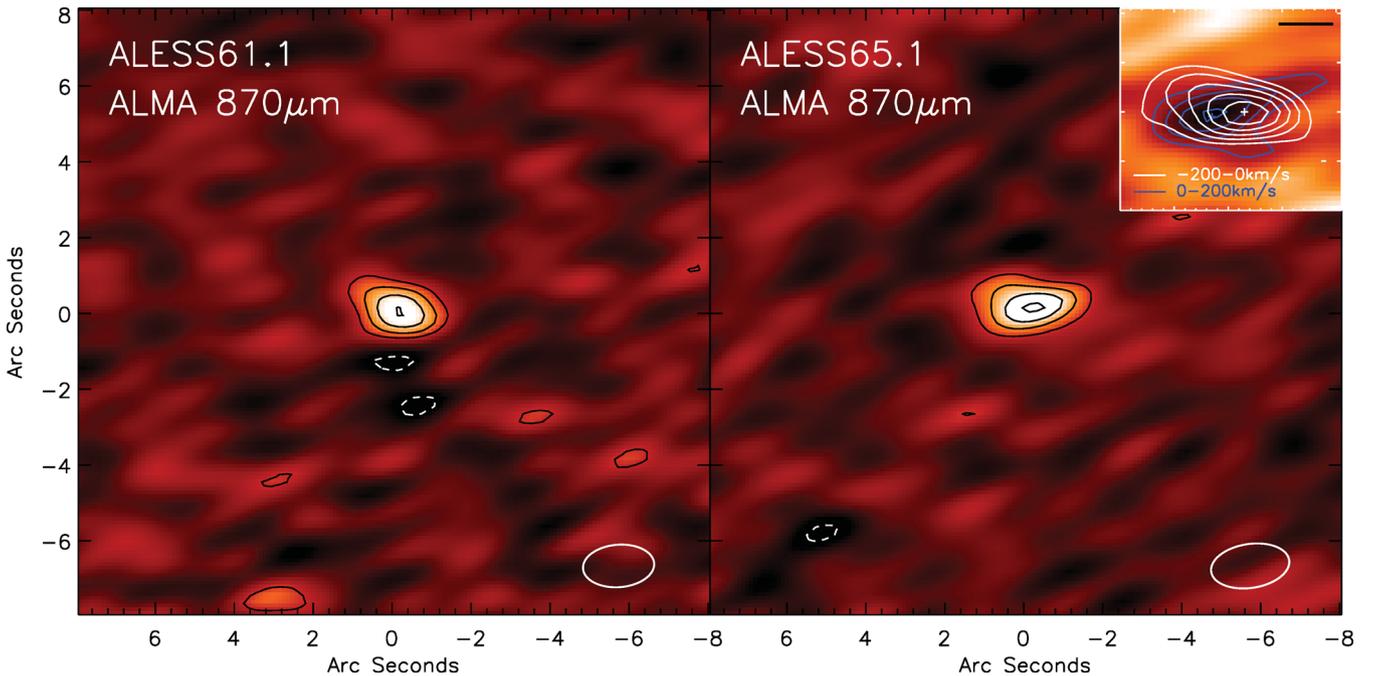
Figure 1. Top: 870-μm (345-GHz) velocity-integrated ALMA maps of LESS 61 and LESS 65 from the Band 7 ALMA observations in compact configuration (these maps include the continuum and emission lines and are naturally weighted). In both cases, we detect strong 870-μm emission in both submillimetre sources associated with a single SMG. The rms noise in these maps is 0.44 and 0.42 mJy beam^{-1} for LESS 61 and LESS 65, respectively. Contours denote $\pm3, 5, 7,...,\sigma$. In each panel, we also show the 50 per cent contour of the synthesized beam which is approximately 1.8×1.2 arcsec^2 in both cases. These maps are centred at α: 03 32 45.87, δ: -28 00 23.3 and α: 03 32 52.26, δ: -27 35 26.3 for LESS 61 and LESS 65, respectively (Table 1). The inset in LESS 65 shows the velocity structure in [C II] in this source. The colour scale shows the (continuum-subtracted) velocity-integrated cube between -210 and 0 km s^{-1} with the blue contours at 2, 3, 4, 5,...,σ. The white contours denote the velocity-integrated emission 0–210 km s^{-1} (also at 2, 3, 4, 5,...,σ). The spatial offset between the blueshifted and redshifted emission in these two images is 0.50 ± 0.25 arcsec (3.3 ± 1.7 kpc). If this spatial and velocity offsets represent rotating gas reservoir, then we estimate a dynamical mass of $M_{\mathrm{dyn}} \sim 3.5 \times 10^{10} \sin^2(i)\,\mathrm{M}_\odot$. In this inset, the solid bar shows a scale of 1 arcsec.
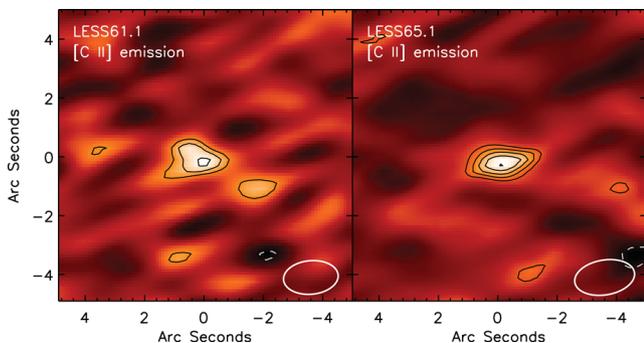
Figure 2. Continuum-subtracted [C II] emission-line maps of LESS 61.1 and LESS 65.1. These are generated by subtracting the continuum and then integrating the cube within ± 2 times FWHM of the emission line. In all panels the contours denote S/N levels denote $\pm 3, 4, 5, \ldots, \sigma$.
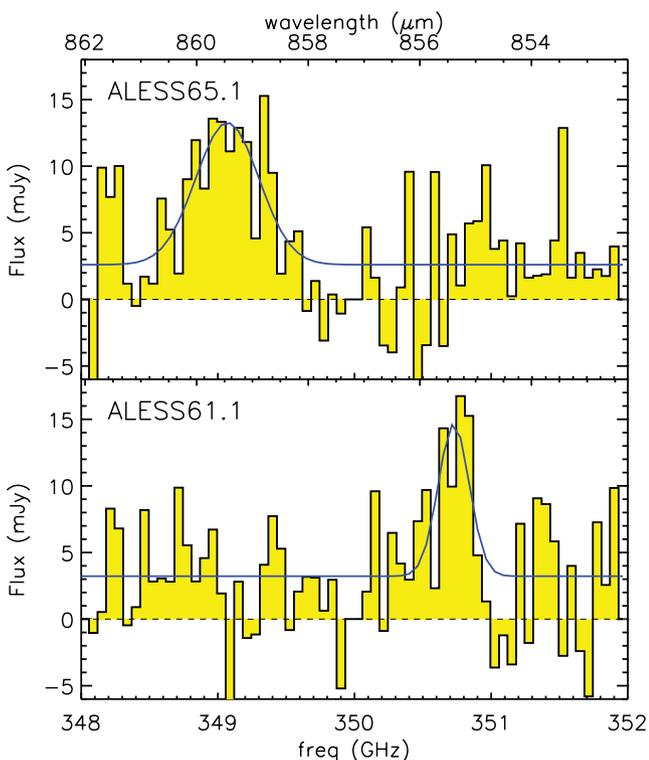
Figure 3. ALMA spectra of ALESS 61.1 and ALESS 65.1, extracted at the position of the peak submillimetre emission from the SMGs. From the spectra, we identify bright emission lines in the upper sideband which we attribute to [C II] emission at $z = 4.419$ and 4.445 for ALESS 61.1 and ALESS 65.1, respectively. The rest-frame equivalent widths of the lines are 0.44 ± 0.06 and $1.12 \pm 0.15\,\mu m$ for ALESS 61.1 and ALESS 65.1, respectively, similar to the median equivalent width of [C II] in local LIRGs and ULIRGs ($W_{o,[C II]} = 0.76 \pm 0.06\,\mu m$; Brauher et al. 2008). In both cases, due to their selection both SMGs have significant continuum emission.

integrating the continuum-subtracted cube over ± 2 times FWHM of the emission line.

In both cases, the LABOCA 870-μm source is identified with a single high signal-to-noise ratio (S/N ~ 8) ALMA SMG in the velocity-integrated maps that is located to within <0.2 arcsec (after centroiding) and 3–4 arcsec from their nominal LABOCA positions (Weiß et al. 2009). Biggs et al. (2011) could not identify robust or tentative counterparts for either of these submillimetre sources (see also Wardlow et al. 2011) as no SMGs were detected at

Table 1. Coordinates and photometry.

	ALESS 61.1	ALESS 65.1
ID[a]	J033245.6−280025	J033252.4−273527
RA (ALMA)[b]	03 32 45.87	03 32 52.26
Dec. (ALMA)[b]	−28 00 23.3	−27 35 26.3
S_{870} (LABOCA)	5.8 ± 1.2	5.9 ± 1.2
S_{870} (ALMA)[c]	4.32 ± 0.44	4.24 ± 0.49
0.365 μm	$<1.2 \times 10^{-4}$	$<9.9 \times 10^{-5}$
0.350 μm	$<9.9 \times 10^{-5}$	$<9.9 \times 10^{-5}$
0.460 μm	$<5.7 \times 10^{-5}$	$<1.8 \times 10^{-4}$
0.538 μm	$<6.9 \times 10^{-5}$	$<3.6 \times 10^{-4}$
0.651 μm	$<6.3 \times 10^{-5}$	$<6.3 \times 10^{-5}$
0.833 μm	$4.7 \pm 1.1 \times 10^{-4}$	$<1.2 \times 10^{-3}$
0.850 μm	$8.5 \pm 1.0 \times 10^{-4}$	$<3.6 \times 10^{-4}$
0.903 μm	$7.3 \pm 1.6 \times 10^{-4}$	$<2.4 \times 10^{-3}$
2.2 μm	$3.0 \pm 0.3 \times 10^{-3}$	$<2.7 \times 10^{-3}$
3.6 μm	$3.3 \pm 0.3 \times 10^{-3}$	$2.1 \pm 0.2 \times 10^{-3}$
4.5 μm	$3.9 \pm 0.2 \times 10^{-3}$	$1.4 \pm 0.2 \times 10^{-3}$
5.8 μm	$2.7 \pm 1.0 \times 10^{-3}$	$1.4 \pm 1.0 \times 10^{-3}$
8.0 μm	$5.4 \pm 0.7 \times 10^{-3}$	$3.0 \pm 0.8 \times 10^{-3}$
24 μm	0.036 ± 0.002	<0.006
250 μm	4.3 ± 1.5	<2.7
350 μm	7.4 ± 1.6	7.6 ± 1.4
500 μm	10.2 ± 1.7	10.2 ± 1.5
1.4 GHz	<0.025	<0.025

Note. All flux densities are in mJy and all limits are 3σ.
[a]LESS ID from the LABOCA catalogue in Weiß et al. (2009).
[b]Coordinates in J2000.
[c]The ALMA flux densities have been primary beam corrected (the primary beam corrections are a factor of 1.12 and 1.04 for ALESS 61.1 and ALESS 65.1, respectively). The *BVRIzK*+IRAC photometry comprises VIMOS (*U*), Multiwavelength Survey by Yale-Chile (MUSYC) (*BVRIz*), *HST* (z_{850LP}), HAWK-I (*K*) and IRAC 3.6–8 μm imaging (see Wardlow et al. 2011, for details). The *Herschel*/SPIRE photometry is measured using archival imaging and the photometry has been deblended for nearby sources. The radio flux density limits are taken from the Very Large Array 1.4-GHz imaging used in Biggs et al. (2011).

1.4 GHz ($3\sigma \le 25\,\mu Jy$ at 1.4 GHz). Both sources are very faint in the *Herschel*/Spectral and Photometric Imaging Receiver (SPIRE) imaging at 250, 350 and 500 μm (the SMGs are weakly detected after deblending nearby sources using the 24 μm and radio as priors; Table 1). The ALMA maps reveal that ALESS 61.1 is associated with a weak 24-μm source that is also visible in the optical–mid-infrared, but ALESS 65.1 does not have any counterparts in the optical or near-infrared and is only detected weakly in the *Spitzer* Infrared Array Camera (IRAC) imaging. Together, this suggest that these galaxies lie at $z \gtrsim 3.5$ (Wardlow et al. 2011). With the current data, we find no evidence for strong gravitational lensing of either of these galaxies.

3.2 Line identification

If the emission lines we identified are indeed [C II], then our data indicate redshifts of $z = 4.419$ and 4.445 for ALESS 61.1 and ALESS 65.1, respectively. The rest-frame equivalent widths of the emission lines are 0.44 ± 0.06 and $1.12 \pm 0.15\,\mu m$, similar to the median equivalent width of [C II] in local LIRGs and ULIRGs ($W_{o,[C II]} = 0.76 \pm 0.06\,\mu m$; Brauher et al. 2008). We note that in the 7.5-GHz spectral coverage at 345 GHz, the emission lines contribute 10–40 per cent of the continuum emission in the velocity-integrated cubes, as predicted by Smail et al. (2011).

We caution that there are other possible identifications for these lines. In particular, the emission could also be [O I] 145 μm ($z \sim 4.9$), [N II] 122 μm ($z \sim 6.0$), [N II] 205 μm ($z \sim 3.1$) or much higher redshift, [O III] 88 μm ($z \sim 8.1$). However, the luminosities of these fine-structure lines are expected to be a factor of $\gtrsim 10$ times fainter than the [C II] emission (e.g. Brauher et al. 2008; Walter et al. 2009b; Decarli et al. 2012; Nagao et al. 2012).

Alternatively, the emission line could also be high-J ^{12}CO at lower redshift (i.e. $z = 1.3$, 1.6, 2.0 and 2.3 for $J = 7$, 8, 9 and 10, respectively). However, the implied emission-line luminosities ($L = 1\text{–}7 \times 10^8 \, L_\odot$) are a factor of ~ 10 times higher than the ^{12}CO line luminosities of any local or high-redshift starbursts or AGN. For example, Mrk 231 has a maximum ^{12}CO luminosity (across all ^{12}CO lines) of $\lesssim 3 \times 10^7 \, L_\odot$ (van der Werf et al. 2010), whilst APM 08279, a well-studied high-redshift far-infrared luminous quasi-stellar object (QSO) has a ^{12}CO(9–8) luminosity $L_{CO} \lesssim 1 \times 10^8 \, L_\odot$. Moreover, if the line high-J ^{12}CO (presumably therefore a galaxy with an AGN), then the gas temperature must be high ($\gtrsim 300$ K if the ^{12}CO spectral line energy distribution peaks beyond $J = 7$). Yet the characteristic dust temperature would have to be $\lesssim 15\text{–}25$ K (for a dust emissivity of $\beta = 1.5\text{–}2.0$). In addition, if these SMGs are lower redshift ($z \sim 1\text{–}3$) starbursts or AGN, then these SMGs also lie significantly off the far-infrared–radio correlation (Condon, Anderson & Helou 1991; Ivison et al. 2010a).

Taken together, we suggest that the line is most likely a fine-structure transition, and given the brightness and equivalent width, probably [C II]. We note that although the redshifts of these two sources are similar ($\Delta v \sim 1500 \, \text{km s}^{-1}$), they are separated by 25 arcmin on the sky (physical distance of 10 Mpc) and so are not physically associated.

3.3 Broad-band spectral energy distribution

We show in Fig. 4 the observed broad-band SED for both galaxies. We overlay the SED of the well-studied $z = 2.3$ starburst SMM J2135−0102 (Ivison et al. 2010b; Swinbank et al. 2010) redshifted to $z = 4.4$ and normalized to the 870-μm photometry. This demonstrates that at $z \sim 4.4$, the 250-, 350- and 500-μm colours and 1.4 GHz of these galaxies are consistent with the expected colours of $z > 4$ ULIRGs (assuming the properties of ULIRGs at $z > 4$ are the same as those at $z \sim 2$; Capak et al. 2008; Schinnerer et al. 2008; Coppin et al. 2009; Daddi et al. 2009).

We fit a modified blackbody to the far-infrared photometry, deriving estimates of the far-infrared (rest-frame 8–1000 μm) luminosities of $L_{FIR} = (2.1 \pm 0.4) \times 10^{12}$ and $(2.0 \pm 0.4) \times 10^{12} \, L_\odot$, for ALESS 61.1 and ALESS 65.1, respectively (corresponding to star formation rates of $\sim 500 \, M_\odot \, \text{yr}^{-1}$; Kennicutt 1998).

To estimate the near-infrared luminosities of these systems, we use the rest-frame UV–mid-infrared SEDs. We fit elliptical, Sb, single burst and constant star formation rate spectral templates from Bruzual & Charlot (2003) to the 0.3–8 μm photometry (Table 1 and Fig. 4) using HYPER-Z (Bolzonella, Miralles & Pelló 2000) at the known redshift. We allow reddening of $A_V = 0\text{–}5$ in steps of 0.2 and overplot the best-fitting SED models in Fig. 4. We then calculate the rest-frame H-band magnitude (observed 8 μm at $z \sim 4.4$), which is less influenced by young stars than rest-frame UV or optical bands and is relatively unaffected by dust. We derive absolute rest-frame H-band magnitudes of $H_{AB} = -24.8 \pm 0.2$ and -24.2 ± 0.3 for ALESS 61.1 and ALESS 65.1, respectively (Table 2). These are comparable to the average H-band magnitudes for radio-identified submillimetre source counterparts at
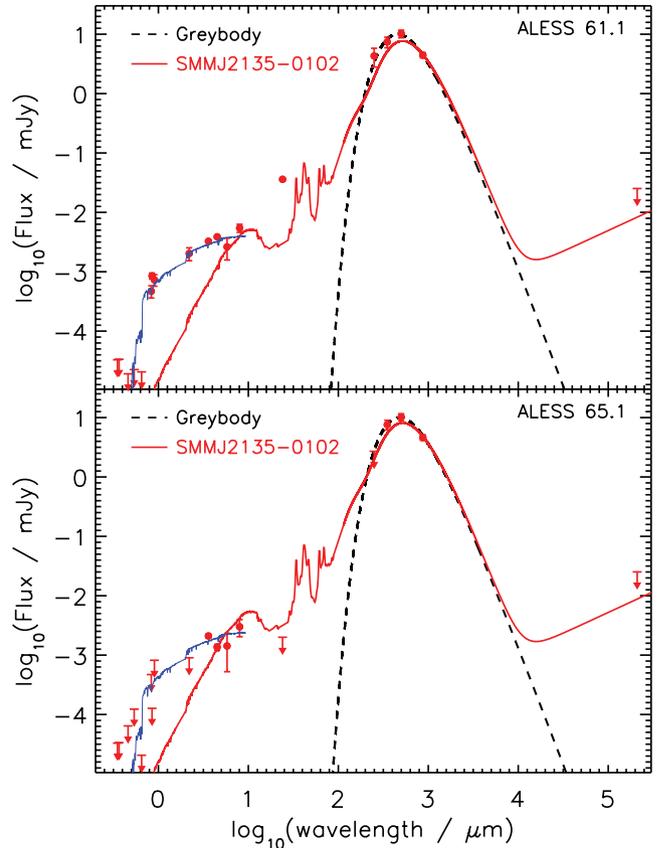
Figure 4. The observed optical–radio SEDs for ALESS 61.1 and ALESS 65.1. We adopt redshifts for the two galaxies of $z = 4.4189$ and 4.4445. We model the far-infrared SEDs using a single-component-modified blackbody dust model (dashed line) by fitting the 250-, 350- and 500-μm limits and 870-μm photometry. We also model the rest-frame UV–near-infrared photometry using HYPER-Z (blue line). The red solid curve show the SED of the well-studied $z = 2.3$ starburst galaxy, SMM J2135, at the redshift of our galaxies (normalized to the 870-μm flux density). This demonstrates that the far-infrared colours are consistent with the high-redshift nature of these galaxies.

Table 2. Physical properties of the galaxies.

	ALESS 61.1	ALESS 65.1
λ_c (μm)	350.726 ± 0.034	349.073 ± 0.032
$z_{[C II]}$	4.4189 ± 0.0004	4.4445 ± 0.0005
$I_{[C II]}$ (Jy km s^{-1})	2.5 ± 0.4	5.4 ± 0.7
FWHM (km s^{-1})	230 ± 25	470 ± 35
$L_{[C II]}$ ($L_\odot$)	$(1.5 \pm 0.3) \times 10^9$	$(3.2 \pm 0.4) \times 10^9$
L_{FIR} ($L_\odot$)	$(2.1 \pm 0.4) \times 10^{12}$	$(2.0 \pm 0.4) \times 10^{12}$
H_{AB}	-24.8 ± 0.2	-24.2 ± 0.3
L_H ($L_\odot$)	$(5.9 \pm 1.0) \times 10^{11}$	$(3.4 \pm 0.8) \times 10^{11}$
$M_\star$ ($M_\odot$)	1.5×10^{11}	9.0×10^{10}

Note. The ALMA data have been primary beam corrected before calculating luminosities. The primary beam corrections are 1.12 and 1.04 for ALESS 61.1 and ALESS 65.1, respectively).

$z \lesssim 3$ ($H_{AB} = -24.1 \pm 0.9$; Wardlow et al. 2011), the bulk of which are expected to be SMGs (Smail et al., in preparation).

Owing to the catastrophic degeneracies between star formation history, age and reddening in SED fitting for dusty sources, to estimate the stellar masses we adopt a simple approach. Following Hainline et al. (2009) and Wardlow et al. (2011) we use the
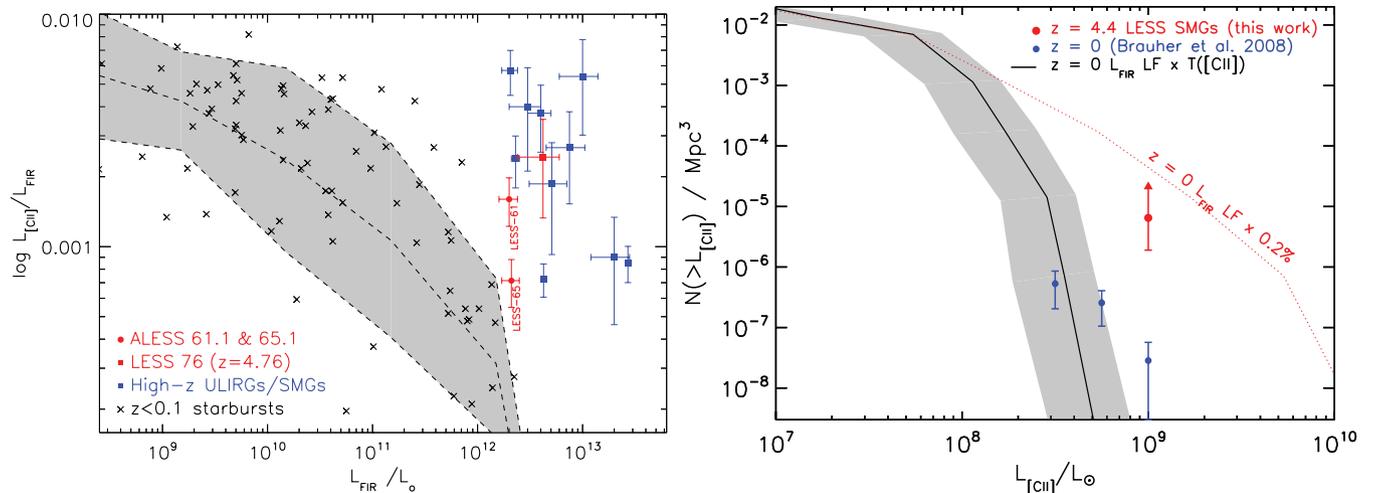
Figure 5. Left: $L_{\text{[C II]}}/L_{\text{FIR}}$ ratio as a function of the far-infrared luminosity for our two $z = 4.4$ ALMA SMGs compared to local star-forming galaxies and ULIRGs. In the plot we also include the $z = 4.76$ LESS SMG from De Breuck et al. (2011; see also Coppin et al. 2009). We also include a number of high-redshift starbursts and AGN from previous studies (Carral et al. 1994; Luhman et al. 1998, 2003; Colbert et al. 1999; Unger et al. 2000; Malhotra et al. 2001; Spinoglio et al. 2005; Brauher et al. 2008; Stacey et al. 2010; Cox et al. 2011). For the local data, we calculate the median (dashed line) and scatter (grey). This figure shows that the ratio of $L_{\text{[C II]}}/L_{\text{FIR}}$ for high-redshift ULIRGs is a factor of $\sim$10 times higher given their far-infrared luminosities compared to those at $z \sim 0$. Right: the [C II] luminosity function at $z = 4.4$ from our survey compared to $z = 0$. For the $z = 4.4$ luminosity function, we assume that all of the [C II]-emitting galaxies in the $\Delta z = 0.12$ volume covered by our observations were detected and so we stress that these calculations yield only a lower limit on the volume density of high-redshift [C II] emitters. The $z = 0$ observations are derived from volume density of *IRAS* sources at $z < 0.05$ from Brauher et al. (2008). The red dotted line shows the predicted [C II] local luminosity function for a constant $L_{\text{[C II]}}/L_{\text{FIR}} = 0.002$, whilst the solid line shows the $z = 0$ far-infrared luminosity function convolved with the $L_{\text{[C II]}}/L_{\text{FIR}}$ function from Brauher et al. (2008) (with the grey region denoting the errors in the volume density of local ULIRGs and scatter in the transfer function). Finding two galaxies in this volume probed by our observations indicates a factor of $\gtrsim$1000 increase in the number density of luminous [C II] emitters from $z \sim 0$ to 4.4, equivalent to an $\sim$3–4 times [C II] luminosity evolution between $z = 0$ and 4.4.

H-band magnitude together with an average mass-to-light ratio for a likely SMG star formation history. Hainline et al. (2009) estimate a *H*-band mass-to-light ratio for SMGs (with burst and constant star formation templates), deriving an average $L_H/M_\star \sim 3.8\,\text{L}_\odot/\text{M}_\odot$ (for a Salpeter initial mass function). This suggests a stellar mass for ALESS 61.1 and ALESS 65.1 of $M_\star \sim 1.5 \times 10^{11}$ and $9^{10}\,\text{M}_\odot$, respectively, comparable to previous estimates for SMG stellar masses (e.g. Hainline et al. 2009; Wardlow et al. 2011). However, we caution that Wardlow et al. (2011) show that the uncertainties in the derived spectral types and ages result in an estimated factor of $\sim$5 times uncertainty in assumed mass-to-light ratios and thus stellar masses.

3.4 The [C II] properties

The [C II] luminosities of our two SMGs, $L_{\text{[C II]}} = 1.5\text{–}3.2 \times 10^9\,\text{L}_\odot$, are comparable to the luminosities of other high-redshift ULIRGs and QSOs (e.g. Maiolino et al. 2009; Walter et al. 2009a; Ivison et al. 2010b; Wagg et al. 2010; De Breuck et al. 2011; Walter et al. 2012). We can crudely estimate the molecular gas mass for these galaxies using the average $\text{[C II]}/{}^{12}\text{CO}(1\text{–}0)$ emission-line ratio ($L_{\text{[C II]}}/L_{\text{CO}(1\text{–}0)} = 4400 \pm 1000$) from a sample of 10 $z = 2\text{–}4$ starbursts (e.g. Hailey-Dunsheath et al. 2010; Ivison et al. 2010b; Stacey et al. 2010; De Breuck et al. 2011), although we caution that there is significant scatter in the CO/[C II] luminosity ratio [e.g. fig. 5 of Stacey et al. (2010) shows that there is a range of $L_{\text{[C II]}}/L_{\text{CO}(1\text{–}0)}$ of approximately 1 dex]. Nevertheless, from this compilation of high-redshift observations, the conversion between [C II] line luminosity and molecular gas mass scales approximately as $M_{\text{gas}} = 10 \pm 2(L_{\text{[C II]}}/\text{L}_\odot)$, suggesting a molecular gas mass for these two SMGs of $M_{\text{gas}} = 1\text{–}4 \times 10^{10}\,\text{M}_\odot$. This molecular gas mass is comparable to the median gas mass implied for SMGs at $z =$

2, $M_{\text{gas}} = 5 \pm 1 \times 10^{10}\,\text{M}_\odot$ (Bothwell et al. 2012). Of course, direct measurements of the low-J CO emission are required to provide a more reliable estimate of the gas mass in these systems.

We can also combine the [C II] and far-infrared luminosities to derive a ratio of $L_{\text{[C II]}}/L_{\text{FIR}} = (7.1 \pm 1.6) \times 10^{-4}$ and $(16.0 \pm 3.7) \times 10^{-4}$ for LESS 61.1 and LESS 65.1, respectively. As Fig. 5 shows, in local luminous star-forming galaxies the ratio of $L_{\text{[C II]}}/L_{\text{FIR}}$ declines by a factor of $\sim$100 over three orders of magnitude in far-infrared luminosity (with a factor of $\sim$3 times scatter at any L_{FIR}). This '[C II] deficit' in local ULIRGs has a number of possible explanations, including enhanced contribution from continuum emission in dusty, high-ionization regions (Luhman et al. 1998, 2003), high-ionization effects in the dense environments (Abel et al. 2009) or enhanced contributions to the infrared luminosity from AGN (Sargsyan et al. 2012).

The ratio we derive for the two $z \sim 4.4$ SMGs is a factor of $\sim$10 times higher than expected for $z \sim 0$ ULIRGs with their far-infrared luminosity (Fig. 5), although the high $L_{\text{[C II]}}/L_{\text{FIR}}$ is similar to other high-redshift galaxies of comparable far-infrared luminosity (e.g. Stacey et al. 2010; Cox et al. 2011; Walter et al. 2012). This has been interpreted as evidence that the molecular emission does not reside in a single, compact region illuminated by an intense UV radiation field (as is a good approximation for local ULIRGs), but rather that the [C II] reservoir is more extended, with the high $L_{\text{[C II]}}/L_{\text{FIR}}$ ratio reflecting the lower density of this extended medium (e.g. Abel et al. 2009; Hailey-Dunsheath et al. 2010; Graciá-Carpio et al. 2011). This interpretation is also consistent with high-resolution studies of SMGs, which have shown that the dust emission and gas reservoirs can be extended over several kiloparsecs (e.g. Biggs & Ivison 2008; Tacconi et al. 2008; Younger et al. 2008; Ivison et al. 2011; Swinbank et al. 2011) and studies of their mid-infrared colours and spectral properties (Menéndez-Delmestre et al. 2007;

Hainline et al. 2009). As we will show in Section 3.5, the [C II] emission in ALESS 65.1 appears to show velocity structure, and we determine that the [C II] reservoir may be extended across $\sim$3 kpc, consistent with this interpretation.

Finally, we note that since the [C II] transition is a primary coolant within the PDRs, it provides a probe of the physical conditions of the gas and interstellar radiation field (e.g. Hollenbach & Tielens 1999; Wolfire et al. 2003). We can therefore use the [C II] and far-infrared luminosity together with the PDR models of Kaufman et al. (1999) to place upper limits on the far-UV radiation field strength and characteristic density of star-forming regions within the ISM. The [C II]/L_{FIR} ratio of our two galaxies, $L_{[C II]}/L_{FIR} = 7.1$–16×10^{-4}, suggests a mean interstellar far-UV radiation field strength $(G) \lesssim 3000$ times that of Milky Way and H$_2$ density $\lesssim 10^{5.5}$ cm^{-3} (e.g. Danielson et al. 2011; see also Hailey-Dunsheath et al. 2010 and Stacey et al. 2010). The far-UV field strength limit derived in this way is comparable to that estimated using STARBURST99, which suggests that a 500 M$_\odot$ yr^{-1} starburst produces a luminosity of $\sim 5 \times 10^{45}$ erg s^{-1} at a wavelength of 1000 Å or a flux density of $\sim 10^{3.5}$ times that of the Milky Way for a source with physical extent of 3 kpc (adopting a far-UV field strength between 912 and 1103 Å for the Milky Way of 1.6×10^{-3} erg s^{-1} cm^{-2}).

3.5 Internal structure

Given the spatial resolution of our observations ($\sim$1.4 arcsec FWHM), we search for spatially resolved emission and velocity structure within these two SMGs. From the ALMA data of LESS 65, the total flux of the galaxy ($S_{870} = 4.24 \pm 0.49$ mJy) is marginally higher than the peak flux in the map ($S_{peak} = 3.60 \pm 0.49$ mJy beam^{-1}), indicating that the source may be marginally resolved. Using the [C II] emission in this galaxy, we examine whether there is any evidence for velocity structure by comparing the spatial distribution of the integrated [C II] emission between -210–0 km s^{-1} and 0–210 km s^{-1} (i.e. $\pm$FWHM relative to the systemic redshift in the continuum-subtracted cube). By centroiding the two maps we derive a spatial offset of 3.3 ± 1.7 kpc between the redshifted and blueshifted emission (Fig. 1). Although tentative, this spatial extent is similar to the [C II] spatial extent of the bright $z \sim 5$ SMG HDF 850.1 where similar data are available (Walter et al. 2012), and also to the high-J ^{12}CO molecular emission FWHM ($\sim$4 kpc) from a sample of eight SMGs at $z \sim 2$ (Tacconi et al. 2006). If the spatial offset in ALESS 65.1 represents rotating gas, then we estimate a mass $M_{dyn} \sim 3.5 \times 10^{10} \sin^2(i)$, which is consistent with the implied gas and stellar mass estimates.

3.6 The evolution of the [C II] luminosity function

Since our ALMA survey has followed up *all* of the LESS SMGs, we can use the detection rate to investigate the evolution of the [C II] luminosity function. In the following we assume that all of the [C II]-emitting galaxies in the $\Delta z = 0.12$ volume covered by our observations were detected and so we stress that these calculations yield only a lower limit on the volume density of high-redshift [C II] emitters.

To estimate the $z \sim 0$ [C II] luminosity function, we start from the $z \sim 0$ far-infrared luminosity function of Sanders et al. (2003) and initially assume a constant $L_{[C II]}/L_{FIR} = 0.002$ (Fig. 5). This provides a firm upper limit to the bright end of $z \sim 0$ [C II] luminosity function, given the observed decline in $L_{[C II]}/L_{FIR}$ at high L_{FIR} (Fig. 5). We can then use the correlation of $L_{[C II]}/L_{FIR}$ with L_{FIR} from Brauher et al. (2008) (see also Fig. 5) to provide a more reliable

estimate. We show our best estimate of the $z \sim 0$ [C II] luminosity function in Fig. 5, including the expected dispersion due to the scatter in the local $L_{[C II]}/L_{FIR}$–L_{FIR} relation.

To assess the reliability of this $z \sim 0$ [C II] luminosity function we attempt to independently derive this using the Brauher et al. (2008) study of [C II] emission in a sample of 227 $z < 0.05$ galaxies from the *ISO* archive. The parent population of this study can be approximated by an *IRAS* 100-μm selected sample at $z < 0.05$ with flux densities between $S_{100\,\mu m} = 1$ and 1000 Jy. There are $\sim$11 000 *IRAS* sources within this redshift and flux density range and so we must account for the incompleteness in the Brauher et al. (2008) sample to derive the $z \sim 0$ [C II] luminosity function. We start by assuming the Brauher et al. (2008) sample is a random subset of the parent population (although we note it is likely that apparently bright sources are over-represented in the sample, and fainter sources correspondingly under-represented). We then only consider *IRAS* sources with flux densities >10 Jy where the fraction of galaxies observed in the Brauher et al. (2008) sample is $\gtrsim$3 per cent of the parent population and then calculate the fraction of galaxies in the Brauher et al. (2008) sample compared to the number of *IRAS* galaxies at $z < 0.05$ in bins of 100-μm flux density and redshift. We use these sampling fractions to correct the apparent [C II] luminosity function within $z < 0.05$ (a comoving volume of 0.035 Gpc^3) and show these data in Fig. 5.

Whilst the local data from Brauher et al. (2008) comprise a complex mix of observations derived from a number of studies, the data are broadly consistent with the bright end of the $z \sim 0$ [C II] luminosity function we derived above from the far-infrared luminosity function and $L_{[C II]}/L_{FIR}$ transfer function.

To place the new ALMA-identified $z = 4.4$ SMGs on this plot, we estimate the volume covered by our observations of Extended *Chandra Deep Field*-South (ECDFS) by considering that the brightest [C II] emitters will correspond to the brightest far-infrared sources (i.e. SMGs). The LESS SMGs are located within a $0°.5 \times 0°.5$ region and assuming our ALMA observations cover [C II] with a redshift range of $\Delta z = 0.12$ at $z \sim 4.4$, we derive a comoving volume of 2.9×10^5 Mpc^3. Finding two galaxies in this volume with [C II] luminosities >1 $\times$ 10^9 L$_\odot$ indicates a factor of $\gtrsim$1000 increase in the number density of luminous [C II] emitters from $z \sim 0$ to 4.4. This is equivalent to an $\sim$3–4 times [C II] luminosity evolution between $z = 0$ and 4.4, which is consistent with the evolution in the far-infrared luminosity function (factor of $\sim$3 times in L_{FIR} for a fixed volume density of $\phi = 10^{-5}$ Mpc^{-1}; Wardlow et al. 2011) between $z = 0$ and 3, although since the far-infrared luminosity function declines beyond $z = 3$, the [C II] luminosity function may peak at lower redshift than probed by our observations here.

4 SUMMARY

We have undertaken an ALMA study of 126 submillimetre sources from the LABOCA 870-μm survey of the ECDFS (Weiß et al. 2009). We focus here on two high-redshift SMGs that are precisely located by our high-resolution ALMA continuum observations and whose ALMA spectra detect bright emission lines. We interpret these lines as the far-infrared atomic fine-structure line [C II] 157.74, indicating redshifts of $z = 4.4$ for both galaxies. We show that the ratio of $L_{[C II]}/L_{FIR}$ is higher than comparably luminous galaxies at $z = 0$, but consistent with the ratio seen in other high-redshift ULIRGs. We interpret this as evidence that the molecular emission is extended and indeed, in one of our SMGs our data suggest that [C II] is resolved on $\gtrsim$3 kpc scales. Given the volume probed by

our observations, we show that the [C II] luminosity function must evolve strongly across the 12 Gyr between $z = 0$ and ~ 4.

These results show that the wide spectral baseline coverage of ALMA provides the opportunity to measure blind redshifts of large samples of distant, obscured galaxies through the detection of fine-structure emission lines, such as [C II], in short exposure times.

REFERENCES

Abel N. P., Dudley C., Fischer J., Satyapal S., van Hoof P. A. M., 2009, ApJ, 701, 1147
Biggs A. D., Ivison R. J., 2008, MNRAS, 385, 893
Biggs A. D. et al., 2011, MNRAS, 413, 2314
Blain A. W., Smail I., Ivison R. J., Kneib J.-P., 1999, MNRAS, 302, 632
Blain A. W., Smail I., Ivison R. J., Kneib J.-P., Frayer D. T., 2002, Phys. Rep., 369, 111
Bolzonella M., Miralles J.-M., Pelló R., 2000, A&A, 363, 476
Bothwell M. S. et al., 2012, MNRAS, submitted
Brauher J. R., Dale D. A., Helou G., 2008, ApJS, 178, 280
Bruzual G., Charlot S., 2003, MNRAS, 344, 1000
Capak P. et al., 2008, ApJ, 681, L53
Carilli C. L., Yun M. S., 2000, ApJ, 530, 618
Carral P., Hollenbach D. J., Lord S. D., Colgan S. W. J., Haas M. R., Rubin R. H., Erickson E. F., 1994, ApJ, 423, 223
Chapman S. C., Smail I., Windhorst R., Muxlow T., Ivison R. J., 2004, ApJ, 611, 732
Chapman S. C., Blain A. W., Smail I., Ivison R. J., 2005, ApJ, 622, 772
Colbert J. W. et al., 1999, ApJ, 511, 721
Condon J. J., Anderson M. L., Helou G., 1991, ApJ, 376, 95
Coppin K. E. K. et al., 2009, MNRAS, 395, 1905
Cox P. et al., 2011, ApJ, 740, 63
Daddi E., Dannerbauer H., Krips M., Walter F., Dickinson M., Elbaz D., Morrison G. E., 2009, ApJ, 695, L176
Danielson A. L. R. et al., 2011, MNRAS, 410, 1687

Dannerbauer H., Lehnert M. D., Lutz D., Tacconi L., Bertoldi F., Carilli C., Genzel R., Menten K., 2002, ApJ, 573, 473
De Breuck C., Maiolino R., Caselli P., Coppin K., Hailey-Dunsheath S., Nagao T., 2011, A&A, 530, L8
Decarli R. et al., 2012, ApJ, 752, 2
Frayer D. T., Smail I., Ivison R. J., Scoville N. Z., 2000, AJ, 120, 1668
Gear W. K., Lilly S. J., Stevens J. A., Clements D. L., Webb T. M., Eales S. A., Dunne L., 2000, MNRAS, 316, L51
Graciá-Carpio J. et al., 2011, ApJ, 728, L7
Hailey-Dunsheath S., Nikola T., Stacey G. J., Oberst T. E., Parshley S. C., Bradford C. M., Ade P. A. R., Tucker C. E., 2008, ApJ, 689, L109
Hailey-Dunsheath S., Nikola T., Stacey G. J., Oberst T. E., Parshley S. C., Benford D. J., Staguhn J. G., Tucker C. E., 2010, ApJ, 714, L162
Hainline L. J., Blain A. W., Smail I., Frayer D. T., Chapman S. C., Ivison R. J., Alexander D. M., 2009, ApJ, 699, 1610
Hollenbach D. J., Tielens A. G. G. M., 1999, Rev. Mod. Phys., 71, 173
Ivison R. J., Harrison A. P., Coulson I. M., 1998, A&A, 330, 443
Ivison R. J. et al., 2002, MNRAS, 337, 1
Ivison R. J. et al., 2007, MNRAS, 380, 199
Ivison R. J. et al., 2010a, A&A, 518, L31
Ivison R. J. et al., 2010b, A&A, 518, L35
Ivison R. J., Papadopoulos P. P., Smail I., Greve T. R., Thomson A. P., Xilouris E. M., Chapman S. C., 2011, MNRAS, 412, 1913
Kaufman M. J., Wolfire M. G., Hollenbach D. J., Luhman M. L., 1999, ApJ, 527, 795
Kennicutt R. C., 1998, ARA&A, 36, 189
Le Floc'h E. et al., 2009, ApJ, 703, 222
Lindner R. R. et al., 2011, ApJ, 737, 83
Lord S. D. et al., 1996, A&A, 315, L117
Luhman M. L. et al., 1998, ApJ, 504, L11
Luhman M. L., Satyapal S., Fischer J., Wolfire M. G., Sturm E., Dudley C. C., Lutz D., Genzel R., 2003, ApJ, 594, 758
McMullin J. P., Waters B., Schiebel D., Young W., Golap K., 2007, in Shaw R. A., Hill F., Bell D. J., eds, ASP Conf. Ser. Vol. 376, Astronomical Data Analysis Software and Systems XVI. Astron. Soc. Pac., San Francisco, p. 127
Madden S. C., Geis N., Genzel R., Herrmann F., Jackson J., Poglitsch A., Stacey G. J., Townes C. H., 1993, ApJ, 407, 579
Maiolino R. et al., 2005, A&A, 440, L51
Maiolino R., Caselli P., Nagao T., Walmsley M., De Breuck C., Meneghetti M., 2009, A&A, 500, L1
Malhotra S. et al., 2001, ApJ, 561, 766
Menéndez-Delmestre K. et al., 2007, ApJ, 655, L65
Nagao T., Maiolino R., De Breuck C., Caselli P., Hatsukade B., Saigo K., 2012, A&A, 542, L34
Pope A. et al., 2006, MNRAS, 370, 1185
Sakamoto K. et al., 2008, ApJ, 684, 957
Sanders D. B., Mirabel I. F., 1996, ARA&A, 34, 749
Sanders D. B., Mazzarella J. M., Kim D.-C., Surace J. A., Soifer B. T., 2003, AJ, 126, 1607
Sargsyan L. et al., 2012, ApJ, 755, 171
Schinnerer E. et al., 2008, ApJ, 689, L5
Smail I., Swinbank A. M., Ivison R. J., Ibar E., 2011, MNRAS, 414, L95
Smolčić V. et al., 2012, ApJS, 200, 10
Spinoglio L., Malkan M. A., Smith H. A., González-Alfonso E., Fischer J., 2005, ApJ, 623, 123
Stacey G. J., Geis N., Genzel R., Lugten J. B., Poglitsch A., Sternberg A., Townes C. H., 1991, ApJ, 373, 423
Stacey G. J., Hailey-Dunsheath S., Ferkinhoff C., Nikola T., Parshley S. C., Benford D. J., Staguhn J. G., Fiolet N., 2010, ApJ, 724, 957
Swinbank A. M. et al., 2010, Nat, 464, 733
Swinbank A. M. et al., 2011, ApJ, 742, 11
Tacconi L. J. et al., 2006, ApJ, 640, 228
Tacconi L. J. et al., 2008, ApJ, 680, 246
Unger S. J. et al., 2000, A&A, 355, 885
Valtchanov I. et al., 2011, MNRAS, 415, 3473
van der Werf P. P. et al., 2010, A&A, 518, L42

Wagg J., Carilli C. L., Wilner D. J., Cox P., De Breuck C., Menten K., Riechers D. A., Walter F., 2010, A&A, 519, L1

Walter F., Riechers D., Cox P., Neri R., Carilli C., Bertoldi F., Weiss A., Maiolino R., 2009a, Nat, 457, 699

Walter F., Weiß A., Riechers D. A., Carilli C. L., Bertoldi F., Cox P., Menten K. M., 2009b, ApJ, 691, L1

Walter F. et al., 2012, Nat, 486, 233

Wang W.-H., Cowie L. L., Barger A. J., Williams J. P., 2011, ApJ, 726, L18

Wardlow J. L. et al., 2011, MNRAS, 415, 1479

Weiß A. et al., 2009, ApJ, 707, 1201

Wolfire M. G., McKee C. F., Hollenbach D., Tielens A. G. G. M., 2003, ApJ, 587, 278

Younger J. D. et al., 2007, ApJ, 671, 1531

Younger J. D. et al., 2008, ApJ, 688, 59

This paper has been typeset from a TEX/LATEX file prepared by the author.